Spiral wave dynamics under feedback control derived from a variety of sensory domains

On-Uma Kheowan,* Supichai Kantrasiri, and Prapin Wilairat
Department of Chemistry, Mahidol University, Rama 6 Road, Bangkok 10400, Thailand

Ulrich Storb and Stefan C. Müller
Institut für Experimentelle Physik, Otto-von-Guericke-Universität Magdeburg, Universitätsplatz 2, D-39106 Magdeburg, Germany
(Received 11 May 2004; published 29 October 2004)

The dynamics of rigidly rotating spiral waves in a reaction layer with light-dependent excitability is studied by numerical integration of a reaction-diffusion equation system with a feedback control. The feedback signal is derived from sensory domains with different geometries by introducing an algorithm that computes the illumination intensity to be proportional to the average wave activity in these domains. It is shown that the shape and size of the trajectories of the spiral wave tip as well as the stability of the spiral rotation depend sensitively on the choice of the geometry of the sensory domain. The numerically observed effects are complemented by constructing a flow map based on an analysis of the feedback signal.

DOI: 10.1103/PhysRevE.70.046221 PACS number(s): 05.45.−a, 05.65.+b, 47.54.+r

I. INTRODUCTION

The implementation of control strategies to manipulate complex oscillations and spatiotemporal patterns has become a central issue of nonlinear dynamics. Feedback methods provide one of the possible control techniques that yield new modes of spatiotemporal behavior [1,2]. These techniques may be designed in different ways. A feedback is global or nonlocal, in contrast to local techniques, if the control signal represents a sum of contributions from all or many parts of the system. Such feedbacks have been used, for instance, to control spatiotemporal activity in the Pt-catalyzed oxidation of CO [3], suggesting a means for enhancing catalytic efficiency [4], in gas discharges to suppress plasma instabilities [5], in electrochemical systems to influence spatial coupling among different active sites [6], and in semiconductors in connection with charge transport phenomena [7]. Propagating waves [8] and, in particular, spiral waves [9–12] in the Belousov-Zhabotinsky (BZ) reaction [13,14] have also been controlled by using these feedback methods, which points to the possibility of manipulating dynamical patterns in excitable media including excitable biological tissues [15–17]. A recent advance in this direction is the control of seizurelike events in hippocampal brain slices with adaptive electric fields [18]. Thus, the ability to regulate spatiotemporal behavior provides both a means of generating desired dynamical patterns and the tools for probing underlying mechanisms.

In this work we perform a numerical study of rigidly rotating spiral waves subjected to a nonlocal feedback derived from a confined "sensory domain." A time-dependent spatially uniform modulation of the system's excitability is taken to be proportional to the integral light absorption observed within this domain. Of both theoretical and practical interest are the geometrical features of the applied sensory domain on the dynamics of the rotating spirals [9–13]. We apply the feedback with different shapes and sizes of the domain and find a broad spectrum of dynamical responses, including various shapes of the spiral tip trajectories and the switching between their stability properties. A flow map and a bifurcation diagram are constructed in order to analyze the observed phenomena.

II. SIMULATION METHOD

Our computations are performed with the light-sensitive two-variable Oregonator model [19–21], which has been successfully used to describe the dynamics of the photosensitive BZ system by including a flux term $\phi=\phi(t)$ for the light-induced bromide production [21]:

$$\frac{\partial u}{\partial t} = D_u \nabla^2 u + \frac{1}{\epsilon}\left[u - u^2 - (fv + \phi)\frac{(u-q)}{(u+q)} \right], \tag{1}$$

$$\frac{\partial v}{\partial t} = u - v. \tag{2}$$

Here, the variables u and v describe the evolution of the concentration of the autocatalytic species $HBrO_2$ and the oxidized form of the catalyst, respectively. $D_u=1$ is the scaled diffusion coefficient of variable u. The catalyst is assumed to be immobilized in a gel matrix; thus, the variable v does not diffuse in this model ($D_v=0$). The parameters have the values $\varepsilon=0.05$, $q=0.002$, and $f=3.5$, which are kept constant. The computations were performed by an explicit Euler method, using the five-point approximation of the Laplacian on a 384×384 array with a grid spacing $\Delta h=0.5$ s.u. and time step $\Delta t=0.001$ t.u..

The feedback signal is determined by the integral of wave activity taken over the sensory domains, expressed as [22]

$$\phi(t) = \phi_0 + k_{fb}[\tilde{B}(t) - \tilde{B}_0], \tag{3}$$

with

*Author to whom correspondence should be addressed. Electronic mail: scokw@mucc.mahidol.ac.th

$$\widetilde{B} = \int_S u dS, \tag{4}$$

where ϕ_0 is constant (=0.01). Thus, the intensity of the feedback signal is controlled by the coefficient k_{fb} and depends linearly on the integral value $\widetilde{B}$ of the variable u over the domain S. The constant $\widetilde{B}_0$ refers to this integral averaged over one period of a spiral placed in the domain center with constant flux term $\phi(t) = \phi_0$.

III. RESULTS

A single spiral is induced from the equation system (1) and (2) by choosing a special initial condition [23]. The variables u and v are initially set to zero uniformly in the medium. To create a spiral then we introduce a nonuniform distribution of the variables. A superthreshold value $u=1$ is given along a line near the boundary of the excitable medium to induce a propagating wave. After this wave has reached the center of the excitable medium, one-half of the planar wave is erased by resetting $u=v=0$. Subsequently, the open end of the planar wave curls into a spiral wave with its core located near the center of the excitable medium. Without external forcing and with the above chosen parameter values, the spiral wave rotates rigidly around a circular core with a rotation period $T_0=8.2$ t.u. and a wavelength $\lambda=4.1$ s.u.. There is ample evidence [9–11,22] that for this kind of nonlocal feedback a spiral wave core placed initially at the center of the sensory domain is destabilized for the case of a positive coupling constant k_{fb} and starts to drift away from the center, as shown in all of the examples of Fig. 1. A previous systematic study of circular sensory domains has shown that it frequently moves asymptotically on a circular attractor [9].

In our simulations we find how the shape of this type of spiral tip trajectories is transformed when the shape of the sensory domain is varied. For a triangular domain the feedback induces the spiral core to drift away from the domain center and to make a turn on each side with an overall 120° change of the drift direction. Finally it describes a trajectory with an approximately threefold symmetry [Fig. 1(a)]. An increase of the number of corners of the sensory domain results in an increase of the number of turning points of the drift direction, as shown in Figs. 1(b) and 1(c). For a square-shaped domain [Fig. 1(b)], the trajectory describes a square-shaped pathway, which is rotated by about 45° with respect to the domain. A further increase in the number of domain corners to form a pentagon [Fig. 1(c)] produces a trajectory that follows an approximately pentagonal pathway inside the domain. It appears to be almost circular, because the five rounded corners of the domain are only faintly reflected. For perfect symmetry, as for the circular domain in Fig. 1(d), the trajectory describes a circular pathway around the domain.

Exerting some shear on the square-shaped domain causes a transformation of the trajectory from a square to a rhombic pathway, as shown in Figs. 1(e) and 1(f). A further decrease of the acute angle of the rhombus induces the trajectory to form a large oblong excursion around the domain [Fig. 1(g)].

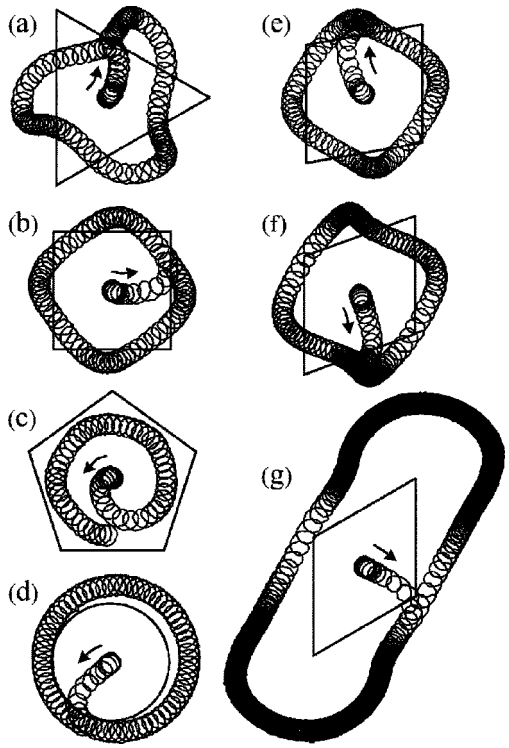

FIG. 1. Trajectories of the spiral wave tip derived from simulations for different shapes of the sensory domain starting from an initial location of the spiral core at the domain center. (a) Triangle, side length 1.50λ, $k_{fb}=0.05$; (b) square, side length 1.00λ, $k_{fb}=0.11$; (c) pentagon, side length 0.75λ, $k_{fb}=0.15$; (d) circle, diameter 1.00λ, $k_{fb}=0.08$; (e)–(g) rhombus, side length 1.00λ and $k_{fb}=0.10$; acute angles: 80°, 70°, and 60°, respectively. The feedback mechanism is computed from Eqs. (3) and (4). Arrows indicate drift direction of the spiral core.

Now the drift velocity of the spiral wave core changes drastically along the oblong pathway. It becomes very slow when the spiral wave core is far away from the center of the rhombic domain. The results demonstrate that the shape of the sensory domain is reflected in the dynamics of the spiral tip trajectory.

Besides the shape of the domain it is also its size that plays a crucial role for the spiral dynamics, as shown in Fig. 2. We use the square-shaped domain with side length d_s to study this effect. For a rather small size ($d_s=0.7\lambda$) one obtains a circular attractor [Fig. 2(a)], not reflecting the fourfold symmetry of the sensory domain. The circular trajectory transforms to a square for $d_s=1.0\lambda$ [Fig. 2(b)], similar to the one in Fig. 1(b). For domains larger than the spiral wavelength the size of the attractor decreases, as shown in Fig. 2(c) where $d=1.25\lambda$.

Note that the drift velocity in Fig. 2(b) is larger than that in Fig. 1(b). This increase is connected with the choice of a larger feedback coupling strength. In fact, we found that for fixed size and shape of the sensory domain larger k_{fb} values lead to a faster drift, as long as the shape of the tip trajectory is rather simple as, for instance, for the case of square domains with size $d_s<1.5\lambda$. For larger d_s the tip dynamics becomes complex (see below) and the influence of k_{fb} cannot be easily predicted.

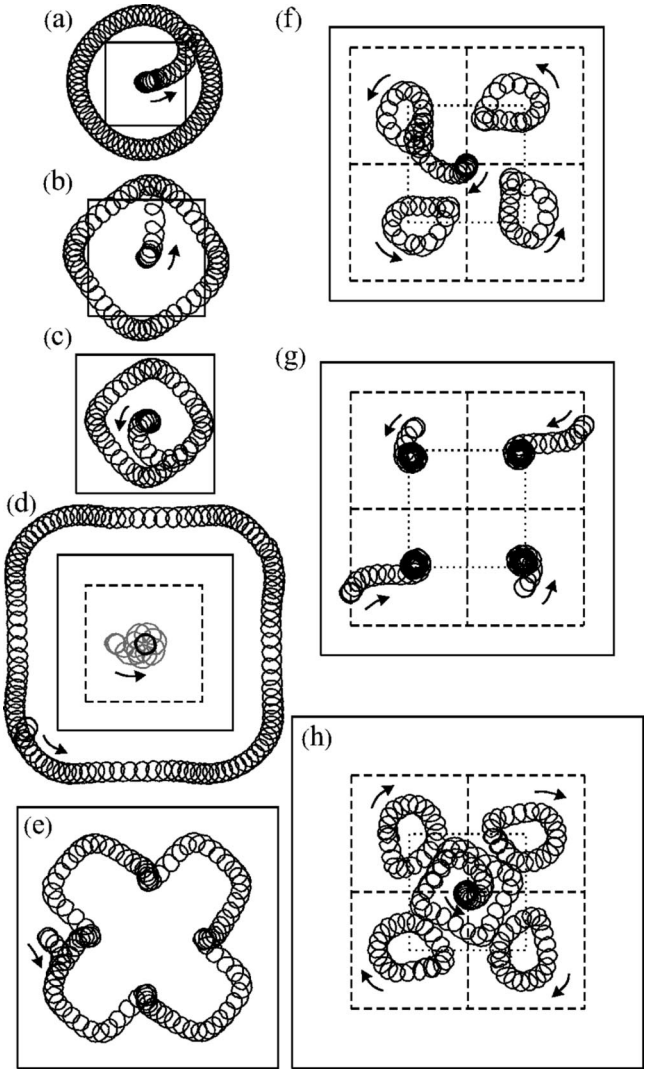

FIG. 2. Trajectories of spiral wave tip under variation of the size of the square domain. (a)–(h) Side length $d_s=0.70\lambda$, 1.00λ, 1.25λ, 1.50λ, 2.25λ, 2.40λ, 2.50λ, 3.00λ; $k_{fb}=0.05$, 0.15, 0.12, 0.20, 0.40, 0.50, 0.50, 0.75. Arrows indicate the drift direction of the spiral core. The dashed squares with $d_s=\lambda$ indicate the approximate location of the separatrix of basins of attraction, whereas the dotted squares depict a reference domain ($d_s=\lambda$). The gray curve in (d) shows the transient trajectory, before a circular, stable rotation is achieved at the center (black circle).

Two trajectories are observed for $d_s=1.50\lambda$ [Fig. 2(d)]. A small, flowerlike trajectory occurs at the center of the domain, when the unperturbed spiral core is initially placed close to the domain center. Note that the gray curve in Fig. 2(d) represents the transient trajectory before a circular, stable rotation (black circle) is achieved at the center. For a larger initial distance to the domain center, the spiral core is attracted towards a trajectory describing a large square with rounded corners. Its orientation coincides with that of the domain, in contrast to the trajectories in Figs. 2(b) and 2(c), which are rotated by about 45° with respect to the domain. The dashed square with side length λ in Fig. 2(d) indicates the approximate location of the separatrix between two basins of attraction that exist for the motion of the spiral core center. However, the attractor, which is eventually reached, is determined not only by the initial location of the spiral core but also by the initial location of the tip with respect to the core center (the initial phase). Thus the location of the separatrix depends on this initial phase, which slightly blurs this separating line. We checked numerically that the blurring effect of the initial phase is below 0.024λ.

An interesting cross-shaped trajectory is created when increasing the domain size to $d_s=2.25\lambda$ [Fig. 2(e)]. This trajectory can be considered as a combination of four small pieces of square-shaped trajectories, which are linked together. With a further increase of d_s to 2.40λ, there appear four trajectories, which are separated from each other [Fig. 2(f)]. Note that the shape of the trajectories changes from a squarelike to a droplike form. Which of these four possible stable orbits is reached depends now on the initial location of the unperturbed spiral core center. The approximate separatrices between the basins of attraction of each orbit are shown by dashed boxes [Fig. 2(f)].

The dynamics of the four attractors in Fig. 2(f) can be stabilized by enlarging the domain to $d_s=2.50\lambda$ [Fig. 2(g)]; the unperturbed spiral wave core is placed at four different locations inside the domain. The feedback induces the spiral wave core to drift towards four stable points (indicated by arrows), located approximately at the corners of the reference domain $d_s=\lambda$ [dotted square in Fig. 2(g)]. At these points, the spiral rotates rigidly without drift. When the domain size is further increased to $d_s=3.00\lambda$, the locations of these four points become again unstable [Fig. 2(h)]; i.e., the spiral wave drifts again along a droplike pathway. Note that the drift direction of these droplike attractors is clockwise and the petals of the loopy trajectories are directed outwards, in contrast to those in Fig. 2(f). In addition, a new square-shaped trajectory with inward directed petals appears around the center of the domain.

The dynamics of the trajectories in Fig. 2 can be divided into two types: stable and unstable spiral rotation. Stable rotation means that the spiral rotates rigidly without drift, as illustrated by the trajectories in Figs. 2(d) (small attractor at the center) and 2(g). All other trajectories in Fig. 2 for which the motion of spiral waves is accompanied by a drift of the spiral wave core are considered as an unstable rotation. These results demonstrate that enlarging the domain size leads to a series of switches from unstable to stable spiral rotation and vice versa.

IV. DISCUSSION

Our discussion is based on the analysis of the integral $\widetilde{B}$ [Eq. (4)] as a function of the rotation angle of spirals placed at different locations inside or outside the square-shaped control domain. It has been shown that the phase of the signal $\widetilde{B}$, which determines the phase of the modulation [Eq. (3)], predominantly affects the drift direction and consequently the shape of the trajectory [12]. The average area under this curve is an appropriate measure for the drift velocity in the range of the sensory domains considered here [12]. The phase relation and the average area form the basis of the flow maps constructed inside and outside the sensory domains as

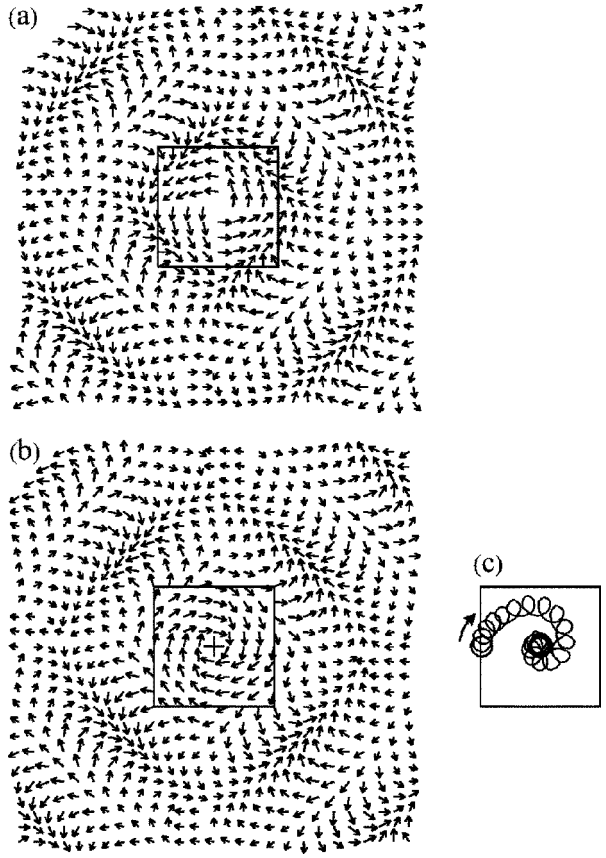

FIG. 3. (a), (b) Vector field plots of the trajectories of the spiral core center under feedback control derived from a square domain with $d_s=\lambda$ for positive feedback (a) and negative feedback (b). (c) Trajectory of the spiral wave tip under negative feedback control with feedback parameters $d_s=1\lambda$ and $k_{fb}=-0.15$. The arrow indicates the drift direction of the spiral core. Note that the coefficient k_{fb} is not involved in the construction of the vectors in the flow map.

shown, for instance, in Fig. 3 for $d_s=\lambda$. The flow vectors observed for positive feedback [Fig. 3(a)], which corresponds to the simulation results observed for $k_{fb}>0$ in Figs. 1(b) and 2(b), are attracted towards two square-shaped trajectories (side length about 1λ and 3λ) on which they are caught in a counterclockwise motion. The flow map unravels the existence of a discrete set of stable square-shaped orbits, which appear to be attractors for the spiral core drift. The innermost trajectory corresponds to the attractor presented in Figs. 1(b) and 2(b). For the flow map observed for negative feedback [Fig. 3(b)], which is obtained by considering the signal $\widetilde{B}$ mirrored with respect to the reference line $B=B_0$ corresponding to negative sign of k_{fb} in Eq. (3), most of the flow vectors inside the domain spiral slowly into the domain center to form a stabilized rotation. This stabilization is confirmed by the simulation result for the tip motion in Fig. 3(c). In a certain region outside the domain the vectors flow towards a square-shaped trajectory with a side length of about 2λ. These flow maps illustrate how the dynamics of the spiral wave can be drastically changed by switching the sign of the feedback gain.

Additional flow maps of the spiral core center under variation of the domain size are shown in Fig. 4. The flow map for the domain with $d_s=1.50\lambda$ is depicted in Fig. 4(a). Here, most of the vectors are attracted towards two types of stable states: a fixed point at the center and a square-shaped orbit in agreement with the trajectories in Fig. 2(d). The basin of attraction of the two states are separated by the separatrix indicated by the dashed square with side length λ. Solid, open, and checked circles in this figure indicate three types of fixed points: (i) the stable node (solid circle), which attracts the vector field from all directions, (ii) the unstable node (open circle), which repels the vector field in all directions, and (iii) the saddle point, which attracts the vector in one direction but repels it in the direction perpendicular to it. For the flow map in Fig. 4(a) there is one stable node located at the center of the domain. It corresponds to the stabilization of rigid rotation and thus to the small attractor in Fig. 2(d). In addition to the stable node at the center of Fig. 4(a), there appear four unstable nodes at the corners and four saddle points on the edges of the reference domain (dashed square).

The flow map for a larger domain ($d_s=2.50\lambda$) is shown in Fig. 4(b). It corresponds to the trajectories in Fig. 2(g). The locations of the four stable nodes in this map coincide with those of the unstable ones for $d_s=1.5\lambda$ [Fig. 4(a)]. Since the distribution of neighboring nodes for each of them is equal to

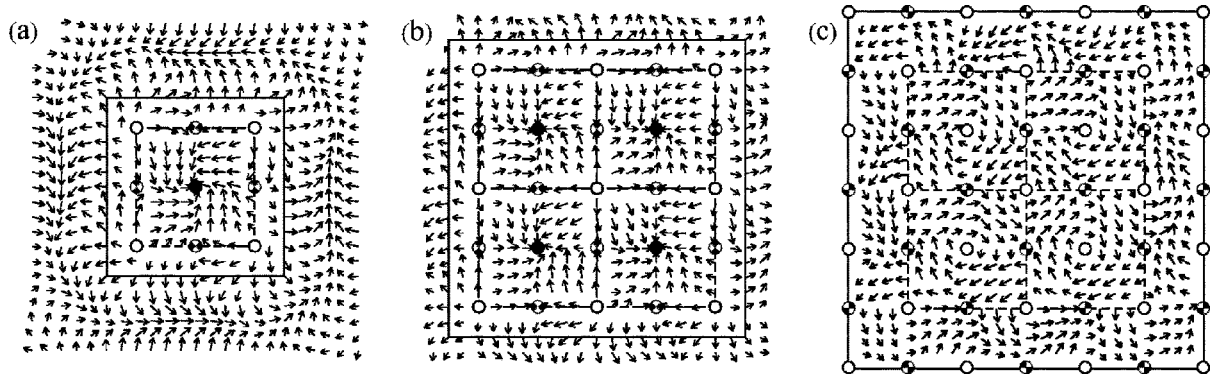

FIG. 4. Flow maps of the spiral core center under variation of the domain sizes for positive feedback, for (a) $d_s=1.50\lambda$, (b) $d_s=2.50\lambda$, and (c) $d_s=3.00\lambda$. Vectors show the drift direction of the spiral core center, which its size indicates the drift velocity. The dashed line indicates the location of the separatrix, which restricts the basin of each attractor. Solid, open, and checked circles indicate the fixed points: stable node, unstable node, and saddle point, respectively.

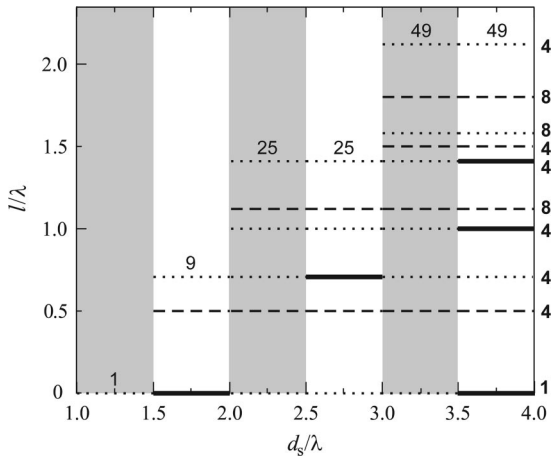

FIG. 5. Bifurcation of the spiral wave rotation under confined-domain feedback control. Number of fixed points inside the sensory domain is illustrated as a function of the normalized size of the domain, d_s/λ. Distance l from the domain center of the fixed point is shown on the y axis. Solid, dashed, and dotted bars indicate the fixed points: stable node, saddle point, and unstable node, respectively. Inserted numbers show the total number of fixed points for each range of d_s. Gray bands indicate the range where no stable rotating spirals exist.

that for the case $d_s=1.5\lambda$, we find a fourfold symmetric repetition of the pattern of Fig. 4(a). The stability of the four fixed points is lost when enlarging the domain size by about 0.5λ, as shown in Fig. 4(c) for $d_s=3.0\lambda$. Here, all the fixed points that are stable in Fig. 4(b) become unstable.

The number of fixed points inside the square domain is 9, 25, and 49 for the side lengths $d_s=1.5\lambda$, 2.5λ, and 3.0λ in Figs. 4(a)–4(c), respectively. Note that for domains smaller than 1.5λ, there exists only one unstable fixed point, which is located at the center of the domain, as shown in Figs. 2(a)–2(c) and Fig. 3(a). However, the domain should not be too small—i.e., smaller than the spiral core. Because if such a small domain is located inside the core, there will be no modulation of the signal and consequently no feedback.

The total number of fixed points, F_n, can be described as a function of the the size of the domain d_s according to $F_n=(2n+1)^2$, where $n=[d_s/\lambda-(d_s/\lambda \bmod 1)]$. For example, if $d_s=1.5\lambda$, then $n=1$ and therefore $F_n=9$, as shown in Fig. 4(a). Furthermore, the number of each type of fixed point is expressed as (i) number of stable nodes, $F_{sn}=n^2$, (ii) number of saddle points, $F_{sdn}=2n(n+1)$, and (iii) number of unstable nodes, $F_{un}=(n+1)^2$. One can see clearly that $F_n=F_{sn}+F_{sdn}+F_{un}$. Note that these relationships can be used for $d_s \geqslant 1.5\lambda$. For $d_s<1.5\lambda$, $F_n=F_{un}=1$ as mentioned above.

A bifurcation diagram characterizing the stability of the spiral core drift under a square-domain feedback control is shown in Fig. 5. Stable fixed points exist along the the solid bars in this diagram, whereas the shaded bands indicate the ranges of d_s/λ in which no stable fixed point can be observed. Instead the spiral core moves asymptotically on closed attractive orbits, as previously illustrated for the trajectories evolving from unstable fixed points in Fig. 2 [except for Fig. 2(g) and the small attractor in the middle of Fig. 2(d)]. These properties of these orbits have some analogy to limit cycles in phase space. The number of fixed points increases stepwise with increasing domain size. Focusing on the stable fixed points (solid bars), their number increases as 1, 4, 9,…, corresponding to the relation $F_{sn}=n^2$ mentioned above. In addition, the stability of the fixed points changes also with enlarging the domain. For example, consider the stability of the fixed point located at the center of the domain (distance $l=0$): the dynamics of this point is unstable for $d_s/\lambda<1.5$ and becomes stable for $1.5\leqslant d_s/\lambda<2.0$. For $d_s/\lambda\geqslant 2.0$ it is unstable until $d_s/\lambda\geqslant 3.5$. Note that the saddle points (dashed bars) keep their characteristics with increasing d_s.

V. CONCLUSIONS

Our results demonstrate that the dynamics of the spiral waves under nonlocal feedback control depends sensitively on the geometry, shape and size of the sensory domain, from which the feedback signal is derived. The results in Fig. 1 show that the geometry of the sensory domain is reflected in the shape of the spiral tip trajectory. For a fixed domain shape—e.g., a square—a small increase of the domain size results in a decrease of the trajectory size as seen when comparing Fig. 2(b) with 2(c) and Fig. 2(f) with 2(g). Several shapes of the trajectory can be observed by enlarging the domain. Along the axis of increment of the domain size, the dynamics can be divided into two types, stable and unstable rotation, as shown in Figs. 2 and 5.

An explanation of the numerically observed effects is proposed by using flow maps constructed from the analysis of the feedback signal. The flow maps in Fig. 3 reveal that our feedback forcing leads to the existence of a discrete set of stable square-shaped orbits, which appear to be attractors for the spiral core drift. In addition, the flow maps demonstrate that the local and global dynamics of the spiral wave can be drastically changed by switching the sign of the feedback gain [see Figs. 3(a) and 3(b)]. It is shown that the shape and size of the trajectories of the spiral wave tip, as well as the stability of the spiral rotation, can be changed by varying the size or shape of the sensory domain. We suggest that the feedback method introduced in this work offers an efficient tool for controlling the dynamics of excitable media in biology [15–17].

ACKNOWLEDGMENTS

O.K., S.K., and P.W. thank the Postgraduate Education and Research Program in Chemistry funded by the Royal Thai Government and O.K. thanks the Thailand Research Fund for financial support.

[1] *Handbook of Chaos Control*, edited by H.G. Schuster (Wiley-VCH, Weinheim, 1999).
[2] E. Ott, C. Grebogi, and J.A. Yorke, Phys. Rev. Lett. **64**, 1196 (1990).
[3] S. Jakubith, H.H. Rotermund, W. Engel, A. von Oertzen, and G. Ertl, Phys. Rev. Lett. **65**, 3013 (1990).
[4] J. Wolff, A.G. Papathanasiou, L.G. Kevrekidis, H.H. Rotermund, and G. Ertl, Science **294**, 134 (2001).
[5] Th. Pierre, G. Bonhomme, and A. Atipo, Phys. Rev. Lett. **76**, 2290 (1996).
[6] K. Krischer, J. Electroanal. Chem. **501**, 1 (2001).
[7] G. Franceschini, S. Bose, and E. Schöll, Phys. Rev. E **60**, 5426 (1999).
[8] T. Sakurai, E. Mihaliuk, F. Chirila, and K. Showalter, Science **296**, 2009 (2002).
[9] O.-U. Kheowan, C.K. Chan, V.S. Zykov, O. Rangsiman, and S.C. Müller, Phys. Rev. E **64**, 035201(R) (2001).
[10] O.-U. Kheowan, V.S. Zykov, and S.C. Müller, Phys. Chem. Chem. Phys. **4**, 1334 (2002).
[11] V.S. Zykov, G. Bordiougov, H. Brandtstädter, I. Gerdes, and H. Engel, Phys. Rev. Lett. **92**, 018304 (2004).
[12] O.-U. Kheowan, S. Kantrasiri, C. Uthaisar, V. Gáspár, and S.C. Müller, Chem. Phys. Lett. **389**, 140 (2004).
[13] A.T. Winfree, Science **175**, 634 (1972).
[14] S.C. Müller, T. Plesser, and B. Hess, Science **230**, 661 (1985).
[15] J.M. Davidenko, A.V. Pertsov, R. Salomonsz, W. Baxter, and J. Jalife, Nature (London) **355**, 349 (1992).
[16] M. Dahlem and S.C. Müller, Exp. Brain Res. **115**, 319 (1997).
[17] M. Falcke, Y. Li, J.D. Lechleiter, and P. Camacho, Biophys. J. **85**, 1474 (2003).
[18] B.J. Gluckman, H. Nguyen, S.L. Weinstein, and S.J. Schiff, J. Neurobiol. **21**, 590 (2001).
[19] R.J. Field and R.M. Noyes, J. Chem. Phys. **60**, 1877 (1974).
[20] W. Jahnke and A.T. Winfree, Int. J. Bifurcation Chaos **1**, 445 (1991).
[21] H.J. Krug, L. Pohlmann, and L. Kuhnert, J. Phys. Chem. **94**, 4862 (1990).
[22] V.S. Zykov, A.S. Mikhailov, and S.C. Müller, Phys. Rev. Lett. **78**, 3398 (1997).
[23] V.S. Zykov and S.C. Müller, Physica D **97**, 322 (1996).